Preprints (www.preprints.org) | NOT PEER-REVIEWED | Posted: 4 June 2021 doi:10.20944/preprints202106.0136.v1

Article

An Improved Droop Control Strategy for Grid-connected Inverter Applied in Grid Fluctuation and Inter-harmonics

Wanwan Xu [1], Bin Wang[1], Jiang Liu[1,2*], Da Li[3]

[1] School of Information Science and Engineering, Wuhan University of Science and Technology,Wuhan, Hubei, People's Republic of China;
[2] Engineering Research Center for Metallurgical Automation and Measurement Technology of Ministry of Education, Wuhan University of Science and Technology, Wuhan, Hubei, People's Republic of China;
[3] Shenzhen Hopewind Electric Co., Ltd., Shenzhen, Guangdong, People's Republic of China;
* Correspondence: liujiang@wust.edu.cn; Tel.: 86+027-68862520

Abstract: The droop control is widely used in grid-connected power generation equipment. However, the complex grid environment, especially including frequency fluctuation and inter-harmonics, directly affects the stability and power quality of the grid-connected inverter. This paper presents a novel instantaneous frequency detection method combined with grid current feedback after high-pass filter to complete power stability control and inter-harmonic suppression. The new method can also avoid traditional cumbersome phase-locked loop. Finally, the simulation and experimental results verify the feasibility and effectiveness of the proposed method. The improved droop control has a good dynamic response capability and inter-harmonic suppression capability for both active and reactive power output.

Keywords: Droop control, grid-connected, inter-harmonics, instantaneous frequency detection, incomplete derivation.

Introduction

Droop control has been widely used for microgrid inverter, however, the performance is rarely considered for future power-electronic-based power system. As increasing number of micro-sources with power electronic devices integrated into the grid. Abundant wide frequency signals such as inter-harmonics (not an integer multiple of the fundamental frequency), fundamental fluctuations are injected into power grid [1]. Besides, wind turbines and photo-voltaic units are installed far from load centers, such as offshore wind farms. These weak interfaces have high impedance that have effects on power stability and voltage regulation [2].

In ideal grid voltage conditions, the droop control method assumed the connecting line is inductive and load angle is small. However, in weak grids, the load angle is large, and the connecting line is resistive [3], distorted voltage conditions will be worse such as frequency/ amplitude fluctuates and harmonics at the point of common coupling (PCC) [4]. Power flow of droop control is sensitive to grid frequency [1]. If it is not modified under distorted grid voltage conditions, the grid current would become distorted, and lead to power oscillations [5].

Now quit number of papers focused on solutions of rejecting the disturbance of background distorted voltage. In paper [6] the current loop gain at harmonic frequency is increased, by proportional resonant plus multiple resonant harmonic compensators, to achieve infinite loop gains at target harmonic. In papers [7-8] have proposed grid voltage feed-forward method, for weak grid, grid voltage is replaced by PCC voltage or capacitor voltage when connected into grid through transformer. However, they are appropriate for harmonics but ignored inter-harmonics. Recently, model predictive controller is getting more and more attention [9], whereas, this approach comes at the expense of pronounced computational complexity.

© 2021 by the author(s). Distributed under a Creative Commons CC BY license.

Preprints (www.preprints.org) | NOT PEER-REVIEWED | Posted: 4 June 2021 doi:10.20944/preprints202106.0136.v1

Some improvements to droop control are proposed for system stabilization. In [1] modified droop control loop was proposed to improve the system stability, an optimization based multivariable control design had been proposed in [10], while they all neglected the weak grid condition. A neat and compact multivariable controller manager for weak micro-grids was presented in paper [11], however, it focused on the concept of multivariable damping and synchronizing current control, which had not noticed the different kinds of voltage distorted conditions. Drawback of droop-based control was in island mode, voltage, and frequency of micro-grid changed with loads [12-13]. Existing modified methods are not effective and applicable in an inter-harmonic environment based on droop control.

This paper presents a universal control strategy for micro-grid inverters under distorted grid voltage conditions. When PCC voltage fundamental frequency fluctuation, harmonics/ inter-harmonics conditions take into consideration, a voltage feed-forward strategy based on instantaneous frequency detection and incomplete differential element harmonic current compensation are present for output power stability and current power quality.

The rest of this paper is organized as follows. In Section II, the structure and droop control of micro-grid inverter is revisited, and grid voltage harmonics/inter-harmonics Influence on frequency detection is analyzed. In Section III, improved suppression control Strategies are explained in detail. In Section IV, simulation based on Matlab/Simulink and the experimental in lab results from a 10*KW* three-phase micro-grid inverter are provided to verify the effectiveness of the proposed improved harmonic current suppression control strategy. Finally, Section V concludes this paper.

1. Modeling of grid-connected inverters

1.1. System modeling

The basic topology of AC micro-grid with three phase inverter is shown in Fig.1, this inverter architecture is a convention full-bridge inverter topology, suitable for grid-connected and stand-alone operation in micro-grid. In this architecture, several PV modules connected with DC side, interfaced with the grid through an LCL filter and mode switch. The inverter is controlled by droop control strategy through the space vector pulse width modulator. The main loads laminator heating system and vacuum mixer have characteristics such as high power, intermittent and nonlinear. High power intermittent operation would lead to amplitude and frequency fluctuates of grid side voltage. Three-phase induction heaters would lead to power drops and unbalance of grid voltage. Additional equipment to compensate harmonics, reactive power, or voltage imbalances, will have complex interaction in power-electronic-based power system [14-15].

There is no zero-sequence current in the three-phase three wire grid connected inverter, hence, the system is usually controlled in the static coordinate system, control system structure is shown in Fig.1.

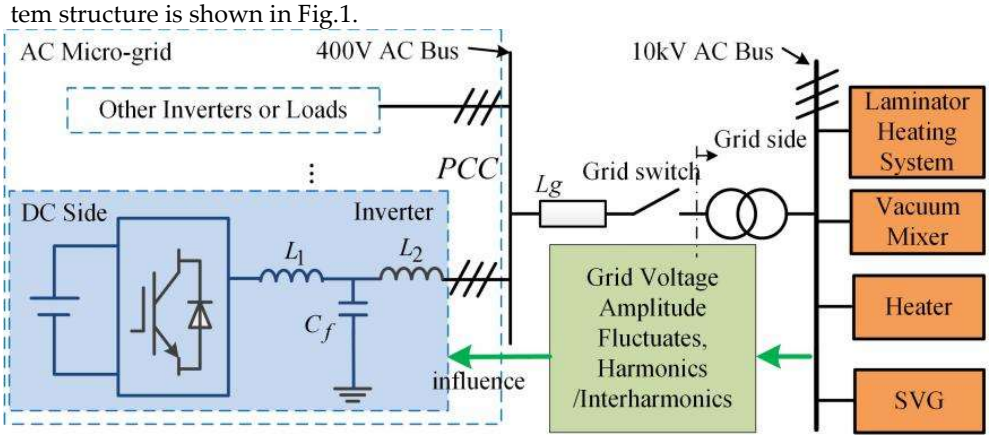

(a)

Preprints (www.preprints.org) | NOT PEER-REVIEWED | Posted: 4 June 2021 doi:10.20944/preprints202106.0136.v1

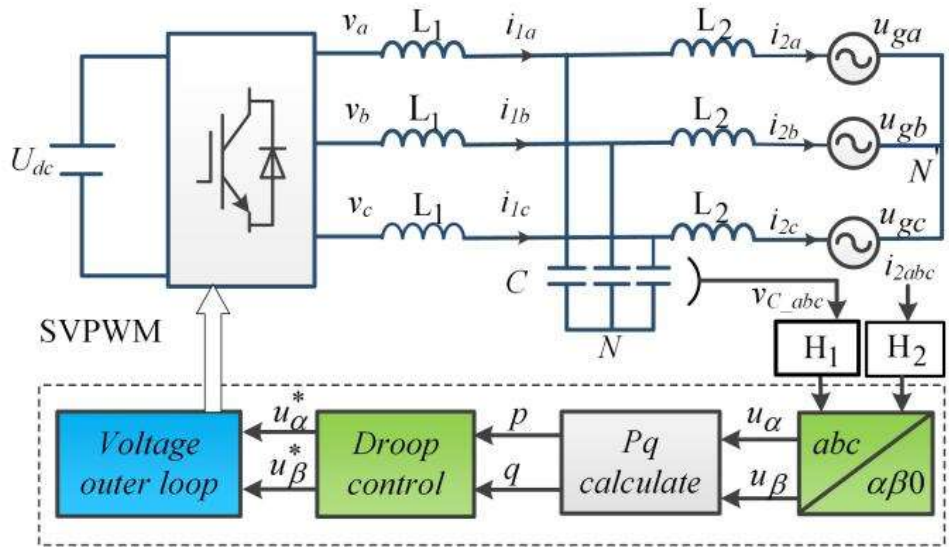

(b)

Fig.1 (a)Topology of AC micro-grid in solar panels factory;(b) Control system structure of inverter in grid-connected mode. (list of symbols is in appendix A)

Droop control method comes from mimic the self-regulation capability of synchronous generator. It is used to adjust frequency and amplitude of V_{ref} according to distribution of P and Q. Assumption the power angle has a small value, the active and reactive powers delivering to grid can be written as [16]:

$$P = \frac{V_{abc}}{R_g^2 + X_g^2}[R_g(V_{abc} - V_g\cos\delta) + X_g V_g \sin\delta) \underset{\delta\to 0}{\overset{R\approx 0}{\approx}} \frac{V_{abc}V_g}{X_g}\sin\delta \tag{1}$$

$$Q = \frac{V_{abc}}{R_g^2 + X_g^2}[X_g(V_{abc} - V_g\cos\delta) - R_g V_g \sin\delta) \underset{\delta\to 0}{\overset{R\approx 0}{\approx}} \frac{V_{abc}(V_{abc} - V_g\cos\delta)}{X_g} \tag{2}$$

Therefore, when inductance X>> resistance R under weak grid, voltage amplitude depends on active power, while frequency is affected by reactive power, then the droop control expression can be written as (3) and (4).

$$f - f_0 = -k_p(P - P_{ref}) \tag{3}$$

$$V - V_0 = k_q(Q - Q_{ref}) \tag{4}$$

As shown in Fig.1(b), the instantaneous active power and reactive power are calculated from the measured-out voltage and current through. Using Clark transformation, $\alpha\beta$ coordinate, and instantaneous power value, the passing through a low-pass filter with cutoff frequency ω_c, P and Q can be obtained as (5).

$$\begin{cases} p = \frac{2}{3}(u_\alpha i_\alpha + u_\beta i_\beta) \\ q = \frac{2}{3}(u_\beta i_\alpha - u_\alpha i_\beta) \end{cases} \tag{5}$$

$$(P,Q) = \frac{\omega_c}{s + \omega_c}(p,q) \tag{6}$$

k_p is droop coefficient; P_0, Q_0 is reference value of active power and reactive power.

In paper [1] small-signal linearizing mode of droop-controlled inverter is manipulated, the results showed active power was less sensitive to fluctuation of grid voltage magnitude, reactive power was more sensitive to fluctuation of grid voltage magnitude

Preprints (www.preprints.org) | NOT PEER-REVIEWED | Posted: 4 June 2021 doi:10.20944/preprints202106.0136.v1

and the former was much higher than the latter. When the droop coefficient k_p is fixed, which means active power keeps a constant sensitivity to grid frequency fluctuation. Therefore, grid fluctuation has a significant impact on power flow control in grid-connected mode.

1.2. Grid voltage harmonics/inter-harmonics Influence on frequency detection

DG units are far away from grid, as a result, grid voltage magnitude and frequency are replaced by filter capacitor voltage through phase-locked loop (PLL). PLL is a process of extracting information about frequency and phase angle of fundamental frequency positive sequence component of grid voltage [17]. The performance of conventional synchronous reference frame phase-locked loop (SRF-PLL) has been widely used [18], Fig.6 shows system of three-phase SRF-PLL. The system consists of a phase-detector, a loop filter, and a digital-controlled oscillator. In presence of non-sinusoidal and unbalance conditions, the problems of Root Mean Square and power measurement is generated remarkable interests in literature [19]. The phase angle extraction of PLL is affected by various disturbances, mainly as unbalanced, harmonic distortion, direct current, frequency variations and inter-harmonics in grid voltage [20].

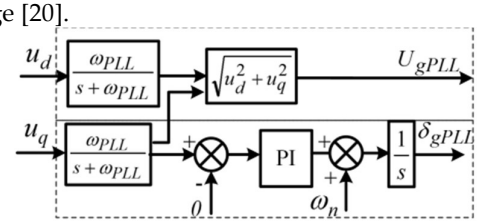

Fig.2 System of three-phase SRF-PLL

In Fig.2, the proportional-integral (PI) controller is used to ensure that the grid voltage vector is perfectly aligned along q-axis. Then added with the nominal frequency of grid and fed to the integrator that acts on frequency error signal and output phase angle value. This phase angle is fed back to transformation block resulting in a closed control loop [21].

Lower band width of SRF-PLL can improve phase estimation accuracy, however it will result in a slow dynamic response under distorted grid conditions [22]. When harmonics fluctuates rapidly, it will unsteady on real-time performance of frequency detection. Bode diagram of SRF-PLL is shown in Fig.3, it shows phase and amplitude decrease in high frequency range. Therefore, high frequency fluctuates cannot be measured by SRF-PLL accurately. Enhanced proportion coefficient can improve rang of detection frequency, however, gain margin decreased as well, which would lead to oscillation [23-24].

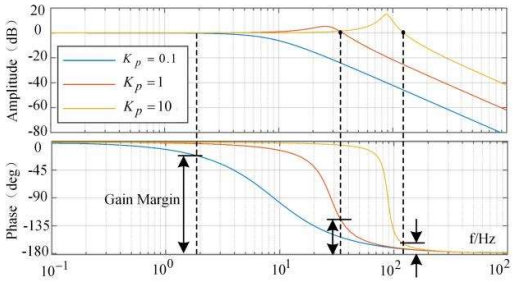

Fig.3 Bode Diagram of SRF-PLL with different k_p

This paper proposes a new method for accurate and fast frequency measurement. The instantaneous frequency can be calculated by the rotating angular velocity of the voltage vector. Fig.4 shows rotation vector diagram of grid side voltage at two adjacent sampling times by Clark transformation.

Preprints (www.preprints.org) | NOT PEER-REVIEWED | Posted: 4 June 2021 doi:10.20944/preprints202106.0136.v1

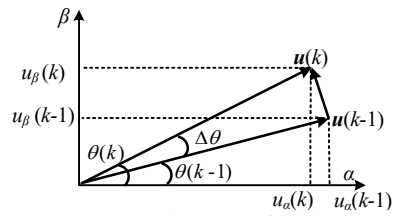

Fig.4 Rotation vector diagram of grid side voltage at adjacent sampling times

Where, *u(k)*, *u(k-1)* are voltage vectors at two adjacent sampling times, *θ(k)*, *θ(k-1)* are voltage vectors angle. *Δt* is sampling time, *m* is maximum harmonic order of grid, instantaneous frequency of voltage can be calculated as:

$$f = \frac{\Delta\theta}{2\pi\Delta t} \approx \frac{\sin\Delta\theta\big|_{\lim\Delta\theta\to 0}}{2\pi\Delta t} = \frac{\sin\theta(k)\cos(k-1) - \cos(k)\sin(k-1)}{2\pi\Delta t} \tag{7}$$

$$\sin\theta(k) = \frac{u_\beta(k)}{|\boldsymbol{u}(k)|} \tag{8}$$

$$\cos\theta(k) = \frac{u_\alpha(k)}{|\boldsymbol{u}(k)|} \tag{9}$$

$$\Delta t \le \frac{1}{2} * \frac{1}{m * 50} \tag{10}$$

2. Improved Suppression control Strategy

2.1. Power stability Control for suppression of grid fluctuation

Some works have been done to develop VVF techniques through two aspects: improving dynamics and self-stability [25] and system electrical damping [26]. The grid voltage cannot be obtained easily for real system, in [26], providing that increasing low-pass filter bandwidth of point of common coupling (PCC) voltage feed-forward method. This paper proposes frequency of voltage based on instantaneous frequency detecting, and grid current feedback control is given by an incomplete derivation with a high-pass filter. The proposed methods are shown in Fig.5.

If the grid voltage contains 280*HZ* inter-harmonics shown in Fig.5(c) u_{abc}, after power calculation, *P* and *Q* also contain 280*Hz* inter- harmonic components, and they cannot be filtered by a low-pass filter.

Preprints (www.preprints.org) | NOT PEER-REVIEWED | Posted: 4 June 2021 doi:10.20944/preprints202106.0136.v1

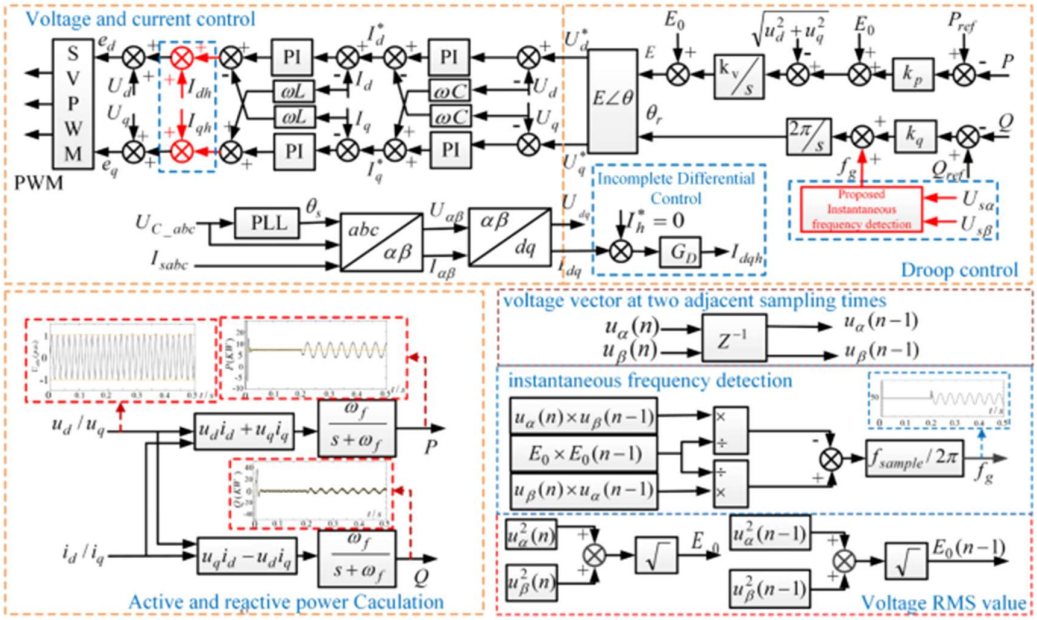

Fig.5, proposed feed-back control strategy

2.2. Harmonic current control loop

After grid voltage orientation is employed, fundamental component of u_{sq} is zero. Thus, the relationship between power and voltage and current in *dq* frame can be expressed as formula (11), P_s^* and Q_s^* are reference of active and reactive power.

$$\begin{cases} I_{sd}^* = P_s^* / U_\alpha \\ I_{sq}^* = Q_s^* / U_\alpha \end{cases} \tag{11}$$

When voltage is harmonically distorted, the α-axis voltage also contains harmonic components. From formula (11), the α-axis current reference contains the same order harmonics as the voltage. The DC component can be restrained by PI regulator, but the harmonic components cannot be restrained due to its limited control band width [27]. The main reason for grid current distorts of inverter connected to grid is a certain degree of the grid voltage, and the output impedance is relatively small. The strategies to suppress the harmonic of grid current are based on increase harmonic impedance and counteract grid harmonic voltage.

Differential control is employed to increase current control gain within a wide harmonic frequency range. However, differential control has potential instability problem as infinite gain at the infinite frequency. Thus, the differential controller is replaced by an incomplete differential element, has been seen in (12). The proposed controller is used to decrease magnitude of harmonic current. H_p is high-pass filter to avoid influence of fundamental frequency that behave as dc components in *dq* frame. Therefore, a second order high-pass filter is more preferable.G_D is to enhance harmonic suppression capability harmonic current T_h^* is set to zero and substrate current, then multiplied with G_D to voltage reference to suppress harmonic current. G_D can be expressed as

$$G_D = H_p H_D = \frac{s^2}{s^2 + 2\xi\omega_n s + \omega_n^2} \frac{ks/\omega_f}{1 + s/\omega_f} \tag{12}$$

Where ξ and ω_n are damping ratio and cutoff frequency of high-pass filter H_p; H_p is used to separate fundamental and harmonic frequency. In this paper, the considered harmonics are between 250*Hz*-1000*Hz*, ξ and ω_n are 0.707 and 500π *rad/s*. H_D is the proposed incomplete differential transfer function, the cutoff frequency ω_f should be higher than harmonic frequency, and it can be set to 10 000π *rad/s*; *k* is control gain.

Preprints (www.preprints.org) | NOT PEER-REVIEWED | Posted: 4 June 2021 doi:10.20944/preprints202106.0136.v1

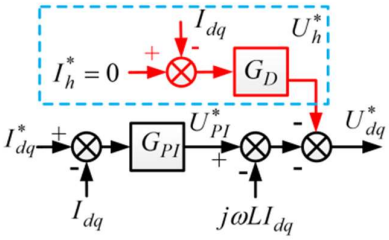

Fig.6 Control block diagram of U_{dq}

Therefore, reference of voltage in dq frame consist of output fundamental frequency controller, decoupling component and output of incomplete differential controller as shown in Fig.6.

Due to three-phase grid connected inverter has the same structure and no coupling term under $\alpha\beta$ frame compared with dq frame. Complete expression of grid-connected current grid- connected current can be derived as.

$$[i_{\alpha\beta}(s)] = \frac{T(s)}{1+T(s)}\frac{1}{H_i(s)}[i_{\alpha\beta}^*(s)] - \frac{G_{x2}(s)}{1+T(s)}[v_{g_\alpha\beta}(s)] \tag{13}$$

$$G_i(s) = \frac{T(s)}{1+T(s)}\frac{1}{H_i(s)} \tag{14}$$

$$G_u(s) = \frac{G_{x2}(s)}{1+T(s)} \tag{15}$$

According to Fig.6, the improved closed-loop transfer function of I_{dq} can be derived as:

$$\begin{aligned} I_{dq} &= YU_{dq} + HI_{dq}^* \\ &\begin{cases} Y(s) = \dfrac{G_u(s)}{1+G_u(s)[G_{PI}(s)+G_D(s)]} \\ H(s) = \dfrac{G_u(s)G_{PI}(s)}{1+G_u(s)[G_{PI}(s)+G_D(s)]} \end{cases} \end{aligned} \tag{16}$$

Where Y is transfer function of current to grid voltage with incomplete differential feed forward control.

Since k of G_D is decisive to harmonic suppression effect, Fig.7 Shows bode diagram of G_D of different k, system parameters are in Table1 in Section IV.

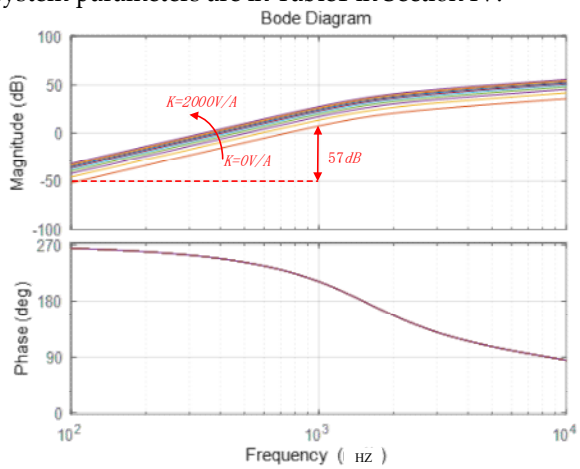

Figure 7. Bode diagram of $G_D(s)$ with different control gains k.

Preprints (www.preprints.org) | NOT PEER-REVIEWED | Posted: 4 June 2021 doi:10.20944/preprints202106.0136.v1

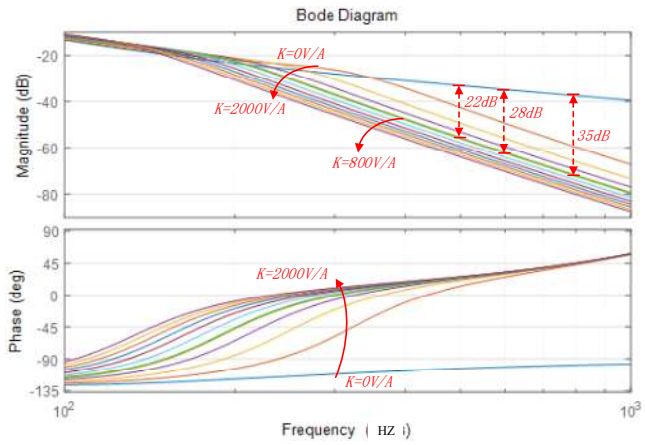

Figure 8. Bode diagram of *Y(s)* with different control gains *k*.

The fundamental frequency in this paper is 50*Hz*.From Fig ,Between 100-1000*Hz*,increasing of *k* can magnify amplitude of G_D, when k=100 *V*/*A* to 2000 *V*/*A*,G_D is -69*dB* and -50*dB* at 50*Hz*, which indicates overlarge may affect control performance at 50*Hz*.In Fig.8,*Y(s)* reflects suppressing capability of harmonics current of the proposed control strategies, when *k*=0, $G_D(s)$=0,it is shown that fundamental control loop has little control ability for harmonic suppression, however, the proposed controller can decrease the amplitude of *Y(s)* significantly, the higher *k* means better harmonic current suppression. According to analysis in Fig.8, *k*=800*V*/*A* is selected for both harmonic suppression and stability performance.

After employing the proposed incomplete differential controller, the close-loop transfer function of *H* in (16) changes. For minimum phase system, the necessary and sufficient conditions for system stability are phase margin is greater than 0 and gain margin is greater than 1. From (16), when *k*=800, gain margin is 13*dB* which can guarantee the stability.

3. Results

The performance of proposed strategies is first verified by simulations in MATLAB/Simulink, and then realized in laboratory. A 10*KW* inverter is adopted. The proposed method is compared against conventional droop control with frequency feed-forward measured by SRF- PLL without grid current feedback.

3.1. Simulation results

According to structure of grid-connected inverter system in Fig.1, main parameters are given in Tab. 1. In order to simulate real system, simulations are care carried out in discrete domain with sample period of 0.1ms, for implementing the discretization of an incomplete differential controller, a pre-warped Tustin transformation is used to convert from s-plane to z-plane.

Preprints (www.preprints.org) | NOT PEER-REVIEWED | Posted: 4 June 2021 doi:10.20944/preprints202106.0136.v1

Tab. 1 Parameters of grid connected inverter system

Parameter	Values
Rated power, frequency	*10KW,50Hz*
LC filter of AC side	*L=1.1mH, C=49μF*
Switching frequency	f_c*=10KHz*
Controller sampling time	$T_C=10^{-4}s$
DC-link voltage	$V_{dc}^*=600V$
Grid nominal voltage (RMS)	$V_g=400V$
Transformer ratio	*n=1:2*
Grid equivalent impedance	*R=2mΩ*
Voltage inner loop coefficient	$K_P=0.1$, $K_i=200$
Droop control coefficient	k_P*=3*10-3,* k_Q*=2*10-4*
incomplete differential controller (G_D)	*k=800,ξ=0.707,*ω_n *=500*π*

Case1: Power stability when the grid voltage frequency fluctuation

Fluctuation of grid voltage fundamental frequency is 1*Hz* and magnitude is 10*V* from 0.2*s* to 0.4*s*, grid voltage consists of 5.6*th* and 7*th* components of 0.0008*p.u*, voltage frequency detection results are shown in Fig.9, compared with SRF and SOGI PLL, the proposed instantaneous frequency detection method keep response time low and high precision.

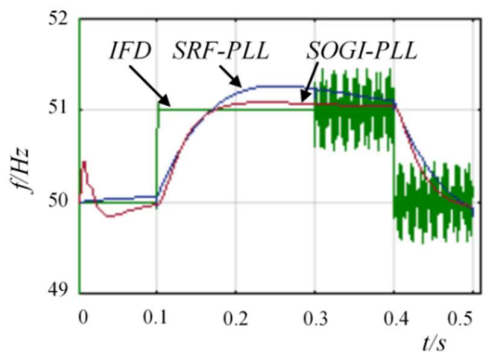

Figure 9. Frequency detection results.

The reference of output active power is set to 6*KW* from 8*KW* at 0.3*s* and reference of reactive power is set from 0 to 2*KW* at 0.3*s*. Fig.10 shows the Simulink results of power stepping under grid voltage frequency fluctuation and harmonics/inter-harmonics. When reference of active power is decrease to 6*KW* from 8*KW*, the output active power cannot be tracked precisely with 1*KW* deviation by conventional droop control strategy. At the same time, it can be seen in Fig.11 that the proposed control strategy reactive respond accurately, it does not worsen dynamic and steady performance of droop control of the inverter system.

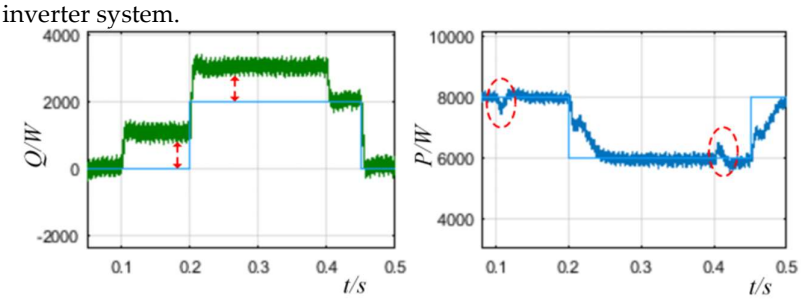

Fig.10 Active and reactive power under grid voltage frequency fluctuation with conventional droop control strategy

Preprints (www.preprints.org) | NOT PEER-REVIEWED | Posted: 4 June 2021 doi:10.20944/preprints202106.0136.v1

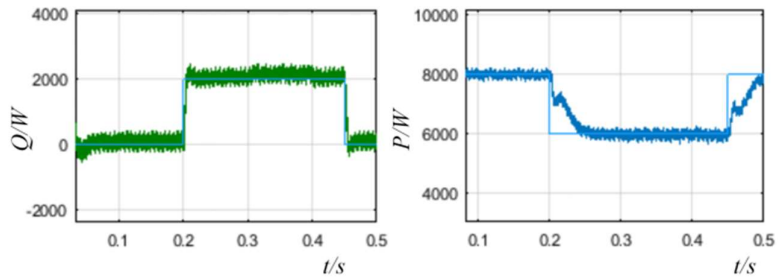

Fig.11 Active and reactive power under grid voltage frequency fluctuation with proposed control strategy

Case2: Current suppression when the grid voltage distorts

Initially, grid voltage fundamental frequency is set to 50*Hz*, fundamental phase voltage is 230*V*.The grid voltage consists of 250*Hz*, 350*Hz*, which are 0.1*p.u.* and 0.1*p.u.* injected at 0.2*s*, and 25*Hz*, 70*Hz*, which are 3.5%, 3.5% injected at 0.35*s*. The grid voltage , frequency and current waveform results from phase A, are shown in Fig,12. The proposed scheme is based on instantaneous frequency detection described in Section III, the traditional scheme is based on SRF-PLL and without incomplete differential element that is k=0 in G_D.

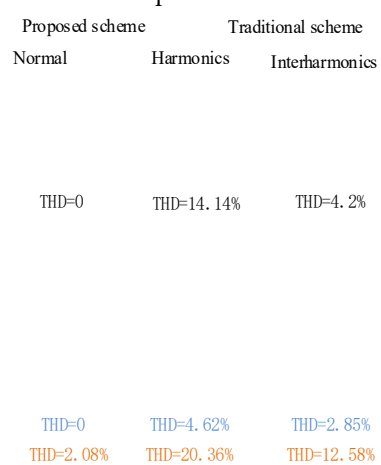

Fig.12 grid voltage waveform, output current of inverter waveform frequency and feed-forward frequency detection results from phase A (measured under *p.u.*) when the grid voltage frequency is 50*Hz*.

From Fig.12, it can be observed that the measured THD of injected grid currents are 4.62% of proposed scheme, that is approximately 1/5 of traditional scheme based on SRF-PLL 20.36% when THD of grid voltage is 14.14%; the measured THD of injected grid currents are 2.85%, that is approximately also 1/5 of traditional scheme based on SRF-PLL 12.58% when THD of grid voltage is 4.2%. The proposed instantaneous frequency detection method can detect power supply voltage frequency changes rapidly. SRF-PLL cannot detect the changes of frequency, and the oscillation time at the beginning is 0.05*s* which is larger than IFD. Therefore, the proposed strategies suppress the injected grid current harmonics and inter-harmonics when the fundamental frequency is stable.

For evaluating the transient response when the fundamental frequency is varied from 46*Hz* to 52.5*Hz* from 0.1*s* to 0.5*s*, the dynamic response is studied. The grid voltage consists of 250*Hz*, 350*Hz*, which are 0.1*p.u.* and 0.1*p.u.* injected at 0.2*s*, and 25*Hz*, 70*Hz*, which are 3.5%, 3.5% injected at 0.35*s*. The grid voltage, frequency and current waveform results from phase A are shown in Fig.13.

Preprints (www.preprints.org) | NOT PEER-REVIEWED | Posted: 4 June 2021 doi:10.20944/preprints202106.0136.v1

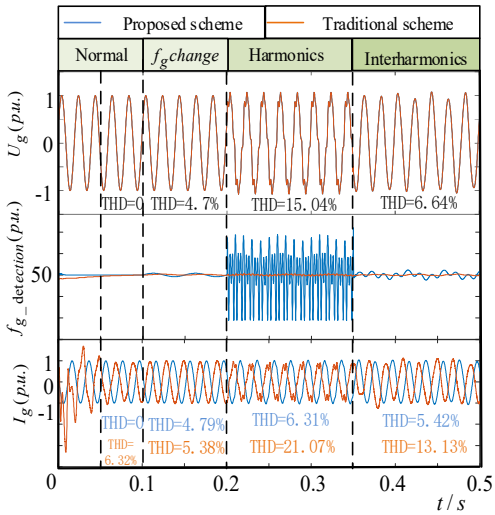

Fig.13 grid voltage waveform, output current of inverter waveform frequency and feed-forward frequency detection results from phase A (measured under *p.u.*) when the grid voltage frequency is varied from 46*Hz* to 52.5*Hz*.

From Fig.13, it can be observed that between 0.1*s* to 0.2*s*, the measured THD of injected grid current is 4.79% of proposed scheme, that is less than traditional scheme based on SRF-PLL 5.38% when fundamental frequency is varied with THD of grid voltage is 4.7%. Between 0.2s to 0.35s. The measured THD of injected grid current is 6.31% of proposed scheme, that is approximately also 1/3 of traditional scheme based on SRF-PLL 21.07% when THD of grid voltage is 15.04%. Between 0.35s to 0.5s, the measured THD of injected grid current is 5.42% of proposed scheme, that is approximately also 1/3 of traditional scheme based on SRF-PLL 13.13% when THD of grid voltage is 6.64%. The proposed strategies can detect power supply voltage frequency variety accurately. SRF-PLL cannot detect the changes of frequency, and the oscillation time at the beginning is 0.05s which is larger than IFD. Therefore, the proposed strategies suppress the injected grid current harmonics and inter-harmonics when the fundamental frequency is varied.

In summary, proposed strategies based on instantaneous frequency detection offers immunity against harmonics and inter-harmonics, whereas the traditional SRF-PLL do not perform accurate. In addition, the dynamic response of proposed scheme is faster than traditional scheme.

3.2. Experimental results

The performance of proposed strategies is further verified through experimental results in laboratory. The algorithm has been designed using TI-DSP28335, voltage and current are sampled by the signal acquisition and conditioning circuit and fed back to the DSP controller, and the DSP calculates the feedback amount to obtain the PWM duty cycle. Since the power of the PWM signal output by the DSP cannot drive the IGBT, it is necessary to add a drive circuit to amplify the power of the PWM signal and isolate the main circuit from the control circuit to protect the control circuit. The IGBT adopts the intelligent switch module IPM. When the IGBT has an over-current fault, it will send a fault signal to the DSP error joint prevention module to prohibit the PWM output.

As shown in Fig.14, grid voltage is simulated by a programmable AC source (AN99030A Ainuo), the proposed strategies are tested on a prototype a two-level PWM inverter. Non-liner load is harmonics/inter-harmonics source. Programmable AC source can change the fundamental frequency and amplitude of the grid.

Experimental results are measured under 3*KW* active power and 2*kVar* reactive power load condition. The simulated grid voltage distorted by 2%, 0.8% of the 5th and 7*th* harmonics and 1% of the 5.8*th* inter-harmonic respectively. The fundamental phase-to phase voltage is 230*V*, the frequency is 50*Hz*, and the frequency changes 0.5*Hz* at 0.4s, and

Preprints (www.preprints.org) | NOT PEER-REVIEWED | Posted: 4 June 2021 doi:10.20944/preprints202106.0136.v1

the rise time is 0.1s. Comparison of output current experimental wave forms between traditional and proposed feed-back control method is shown in Fig15.

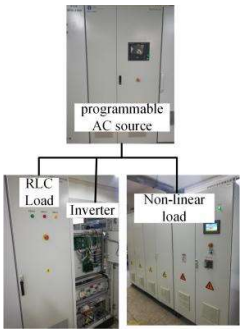

Fig.14 Experimental Prototype developed in the laboratory

From Fig.15(c), a grid voltage fundamental frequency changes from 50Hz to 50.5Hz with harmonics, the corresponding current responses of proposed harmonic current suppression control is observed faster and more stable, compared with traditional feed-back control method. The maximum oscillation value of the current has reached 5A of traditional feed-back control method based on SRF-PLL. The measured total harmonic distortion (THD) of injected grid current is shown in Fig.15(a) and (b), the measured THD of injected grid currents are 13.87% and 3.26% respectively. It can be observed that grid voltage distortion effects injected grid current of micro-gird inverter and the proposed harmonic current suppression control scheme suppress the injected grid current harmonics and inter-harmonics. Compared with traditional feed- forward control method, the proposed strategies have a relatively preferably performance on suppressing the injected grid current harmonics.

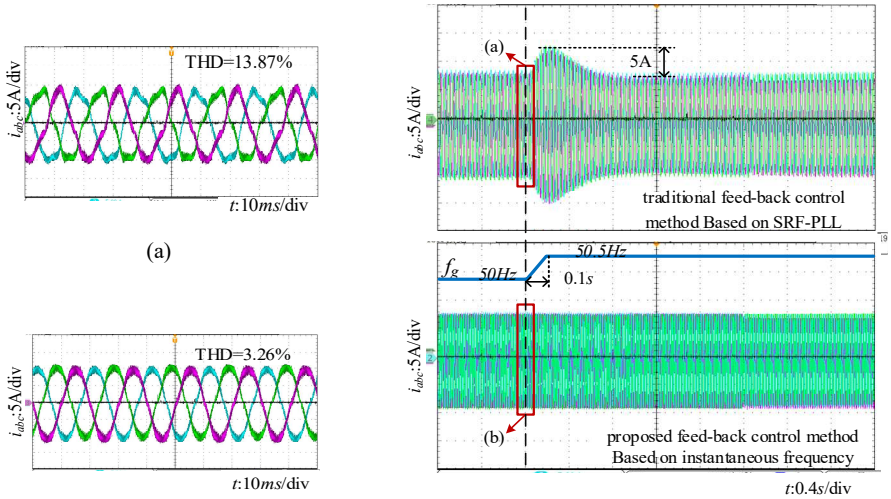

Fig.15 Experimental results of grid current comparison.

5. Conclusions

The improved feed-forward droop control schemes of grid voltage in synchronous d-q frame are proposed in this paper. A novel instantaneous frequency detection is investigated in this paper. A brief comparison between traditional droop control and proposed harmonic current suppression control for LCL-type three-phase grid-connected inverter is presented. It is important to noticed that the traditional droop control based on SRF-PLL frequency detection unable to accurately measure the grid voltage feed-forward frequency under distorted grid. With the proposed harmonic current suppression feed-back control scheme, the injected grid current harmonics and inter- harmonics caused by grid

Preprints (www.preprints.org) | NOT PEER-REVIEWED | Posted: 4 June 2021 doi:10.20944/preprints202106.0136.v1

voltage are greatly reduced. Moreover, under step change of fundamental frequency, the transient response has greatly improved. The advanced performance of the proposed feed-forward control strategies is verified through simulations and experiments.

It is hoped that this work will offer useful reference to improve synchronization frequency detection accuracy and the quality of the injected power from DGs with feed-forward schemes.

Author Contributions: Conceptualization, Wanwan Xu. and Bin Wang; methodology, Wanwan Xu; software, Wanwan Xu and Da Li; validation, Wanwan Xu, Jiang Liu and Da Li; formal analysis, Wanwan Xu; investigation, Wanwan Xu; resources, Bin Wang; data curation, Wanwan Xu; writing—original draft preparation, Wanwan Xu; writing—review and editing, Wanwan Xu; visualization, Jiang Liu.; supervision, Bin Wang; project administration, Bin Wang; funding acquisition, Bin Wang. All authors have read and agreed to the published version of the manuscript.

Funding: The work described in this paper was supported in part by the National Natural Science Foundation of China (No.51877161 to Bin Wang) and Teaching Research Project (No.2020X066 to Wanwan Xu). The authors declare that they have no competing financial interests.

Appendix A

Tab. 1 Definition of symbols in Fig.1

Definition	symbols
Voltage of DC side	U_{dc}
Grid voltage	u_g (V_g as RMS)
Output voltage of Inverter	v_{abc} (V_{abc} as RMS)
Output current of Inverter	i_{2abc}
Conductance and capacity of filter	L_1, L_2, C_f
sampling coefficient	H_1, H_2
Instantaneous active power, reactive power	P, Q
Reference active power, reactive power	P_{ref}, Q_{ref}
Grid equivalent impedance	$L_g=R_g+jX_g$

Data Availability Statement: All data included in this study are available upon request by contact with the corresponding author.

Conflicts of Interest: We declare that we have no financial and personal relationships with other people or organizations that can inappropriately influence our work

References

1. Deng Y, Tao Y, Chen G, et al. Enhanced power flow control for grid-connected droop-controlled inverters with improved stability. IEEE Transactions on Industrial Electronics, vol. 64, no. 7, pp. 5919-5929, July 2017.
2. X. Wu, X. Li, X. Yuan, and Y. Geng. Grid harmonics suppression scheme for LCL-type grid-connected inverters based on output admittance revision. IEEE Transactions Sustain. Energy, vol.6, no.2, pp. 411–421, April 2015.
3. W. Yao, M. Chen, J. M. Guerrero, and Z.-M, Qian. Design and analysis of the droop control method for parallel inverters considering the impact of the complex impedance on the power sharing. IEEE Transactions on Industrial Electronics, vol. 58, no.7, pp. 576–588, Feb 2011.
4. J. Liu, Y. Miura, and T. Ise. Comparison of dynamic characteristics between virtual synchronous generator and droop control in inverter based distributed generators. IEEE Transactions Power Electron. vol.31, no.5, pp. 3600–3611, May 2016.
5. Silwal S, Taghizadeh S, Karimighartemani M, et al. An enhanced control system for single-phase inverters interfaced with weak and distorted grids. IEEE Transactions on Power Electronics, vol.34, no.12, pp.12538-12551, 2019.
6. H. Zhang, X. Ruan, Z. Lin, L. Wu, Y. Ding and Y. Guo, "Capacitor Voltage Full Feedback Scheme for LCL-Type Grid-Connected Inverter to Suppress Current Distortion Due to Grid Voltage Harmonics, IEEE Transactions on Power Electronics, vol. 36, no. 3, pp. 2996-3006, March 2021.
7. Q. Liu, Y. Li, S. Hu, L. Luo, A transformer integrated filtering system for power quality improvement of industrial dc supply system, IEEE Transactions on Power Electronics, vol.67, no.5, pp. 3329–3339, May 2020.

Preprints (www.preprints.org) | NOT PEER-REVIEWED | Posted: 4 June 2021 doi:10.20944/preprints202106.0136.v1

8. Q. Liu, Y. Li, L. Luo, Y. Peng, Y. Cao. Power quality management of PV power plant with transformer integrated filtering method, IEEE Transactions on Power Electronics.vol.34, no.3, pp. 941–949, June 2019.
9. R. S. Alishah, K. Bertilsson, F. Blaabjerg, M. A. J. Sathik and A. Y. Rezaee.New Grid-Connected Multilevel Boost Converter Topology with Inherent Capacitors Voltage Balancing Using Model Predictive Controller. 2020 22nd European Conference on Power Electronics and Applications, 2020, pp. 1-7,
10. B. Bahrani, A. Karimi, B. Ray, and A. Rufer. Decoupled dq-current control of grid-tied voltage source converters using nonparametric models, IEEE Transactions on Power Electronics. vol. 60, no.4, pp. 1356– 1366, April 2013.
11. Ashabani M, Mohamed A R I, Mirsalim M, et al. Multivariable Droop Control of Synchronous Current Converters in Weak Grids/Microgrids With Decoupled dq-Axes Currents. IEEE Transactions on Smart Grid, vol. 6, no.4, pp. 1610-1620,2015.
12. M. Savaghebi, A. Jalilian, J. C. Vasquez and J. M. Guerrero, Secondary Control Scheme for Voltage Unbalance Compensation in an Islanded Droop-Controlled Microgrid, IEEE Transactions on Smart Grid, vol. 3, no. 2, pp. 797-807, June 2012.
13. J.C. Vasquez, M. Guerrero, M. Savaghebi, J. Eloy-Garcia, and R. Teodor escu. Modeling, analysis, and design of stationary-reference- frame droop-controlled parallel three-phase voltage source inverters. IEEE Transactions on Industrial Electronics, vol.60, no.4, pp. 1271–1280,2013.
14. Cavazzana F, Mattavelli, P Corradin M, et al. On the stability analysis of multiple parallel inverters using the impedance multiplication effect. IET Int. Conference on Power Electronics. Glasgow, UK, pp.1–6. April 2016.
15. Chen J, Shao H, Cheng Y, et al. Harmonic circulation, and DC voltage instability mechanism of parallel-SVG system. IET Renewable Power Generation.vol.14, no. 5, pp. 793- 802,2020.
16. Dong D, Wen B, Boroyevich D, et al. Analysis of Phase-Locked Loop Low-Frequency Stability in Three-Phase Grid-Connected Power Converters Considering Impedance Interactions. IEEE Transactions on Industrial Electronics, vol.62, no.1, pp. 310-321,2015.
17. T. Thacker, et al. Phase-Locked Loop Noise Reduction via Phase Detector Implementation for Single-phase Systems. IEEE Transactions on Industrial Electronics, vol.58, pp. 2482-2490,2011.
18. S. Golestan, M. Monfared, and F. D. Freijedo. Design- oriented study of advanced synchronous reference frame phase-locked loops, IEEE Transactions on Power Electronics.vol.28, no. 2, pp. 765–778, Feb 2013.
19. Feola L, Langella R, Testa A. On the Effects of Unbalances, Harmonics and Interharmonics on PLL Systems. IEEE Transactions on Instrumentation and Measurement, vol. 62, no.9, pp.2399-2409,2013.
20. Ali Z, Christofides N, Hadjidemetriou L, et al. Design of an advanced PLL for accurate phase angle extraction under grid voltage HIHs and DC offset. IET Power Electronics, vol.11, no. 6, pp.995-1008, 2018.
21. L. Yang et al. Effect of phase locked loop on small-signal perturbation modeling and stability analysis for three-phase LCL-type inverter connected to weak grid. IET Renewable Power Generation, vol.13, no.1, pp. 86–93, 2018.
22. M. Davari and Y. A. I. Mohamed, Robust Vector Control of a Very Weak-Grid-Connected Voltage-Source Converter Considering the Phase-Locked Loop Dynamics,in IEEE Transactions on Power Electronics, vol. 32, no. 2, pp. 977-994, Feb. 2017.
23. D. Dong, B. Wen, D. Boroyevich, P. Mattavelli and Y. Xue, Analysis of Phase-Locked Loop Low-Frequency Stability in Three-Phase Grid-Connected Power Converters Considering Impedance Interactions, in IEEE Transactions on Industrial Electronics, vol. 62, no. 1, pp. 310-321, Jan. 2015.
24. J. Z. Zhou, H. Ding, S. Fan, Y. Zhang and A. M. Gole, Impact of Short-Circuit Ratio and Phase-Locked-Loop Parameters on the Small-Signal Behavior of a VSC-HVDC Converter, in IEEE Transactions on Power Delivery, vol. 29, no. 5, pp. 2287-2296, Oct. 2014.
25. M. Zhao, X. Yuan, J. Hu and Y. Yan, Voltage Dynamics of Current Control Time-Scale in a VSC-Connected Weak Grid, in IEEE Transactions on Power Systems, vol. 31, no. 4, pp. 2925-2937, July 2016.
26. L. Harnefors. Analysis of sub synchronous torsional interaction with power electronic converters, IEEE Transactions Power System, vol.22, no.1, pp. 305–313,2007.
27. P. Cheng et al. Direct stator current vector control strategy of DFIG without phase-locked loop during network unbalance, IEEE Transactions on Power Electronics, vol. 32, no. 1, pp. 284–29, 2017.